Development of a fluid dynamic gauging method for the characterization of fouling behavior during cross-flow filtration of a wood extraction liquor

Citation for the original published paper (version of record):
Arandia, K., Balyan, U., Mattsson, T. (2021). Development of a fluid dynamic gauging method for the characterization of fouling behavior
during cross-flow filtration of a wood extraction liquor. Food and Bioproducts Processing: Transactions of the Institution of of Chemical Engineers, Part C, 128: 30-40.
http://dx.doi.org/10.1016/j.fbp.2021.04.009

Contents lists available at ScienceDirect

Food and Bioproducts Processing

journal homepage: www.elsevier.com/locate/fbp

Development of a fluid dynamic gauging method for the characterization of fouling behavior during cross-flow filtration of a wood extraction liquor

Kenneth Arandia[a,b], *Upasna Balyan*[a], *Tuve Mattsson*[a,b,*]

[a] *Department of Chemistry and Chemical Engineering, Chalmers University of Technology, SE-412 96 Gothenburg, Sweden*

[b] *Wallenberg Wood Science Center, The Royal Institute of Technology, Chalmers University of Technology, Linköping University, SE-100 44 Stockholm, Sweden*

ARTICLE INFO

Article history:
Received 29 January 2021
Received in revised form 13 April 2021
Accepted 16 April 2021
Available online 21 April 2021

Keywords:
Fluid dynamic gauging
Membrane fouling
Cross-flow filtration
Steam explosion
Wood components

ABSTRACT

A method based on fluid dynamic gauging (FDG) was developed to investigate the membrane fouling behavior of streams containing dissolved wood components and small particles extracted using a mild steam explosion pretreatment. Industrially chipped softwood was subjected to saturated steam at 7 bar for 20 min, followed by cross-flow filtration of steam explosion liquors using 10 kDa polysulfone membranes at 2 bar transmembrane pressure. The results showed a severe decline in permeate flux during the initial stages of the cross-flow filtration. The FDG profiles from five filtration experiments revealed that thicker fouling layers were formed during initial fouling on pristine membranes compared to subsequent fouling on non-pristine membranes. The difference in fouling behavior suggests that cake layer formation was dominant during initial fouling, whereas pore blocking was more pronounced during refouling. This study highlights how FDG can be used to gain a better mechanistic understanding of the fouling behavior of extracted wood components.

1. Introduction

Membrane separation processes are applied in a wide range of industrial sectors, e.g. food processing, pharmaceutical technology, drinking water production and wastewater treatment. Compared to conventional thermal separation processes such as distillation, sublimation and crystallization, membrane separation offers several advantages including a lower energy requirement, lower chemical consumption and higher selectivity (Uragami, 2017). In the pulp and paper industry, membrane operations can facilitate the production of new products from currently underutilized streams containing biomass as industries are shifting toward replacing petroleum-based products with renewable materials. Valuable materials can be recovered from process streams which can contribute to the concept of a "circular economy" by converting lignocellulosic biomass to renewable, bio-based products (Ragauskas et al., 2006). Separation processes must nevertheless be optimized if forest-based biomass are to be utilized efficiently and costs minimized, as separation accounts for a substantial proportion of the total process costs.

The fractionation of dissolved wood components based on their molecular weight as well as the concentration of diluted streams can be performed by membrane ultrafiltration (UF). UF is an attractive separation process for recovering hemicelluloses from mixtures of extracted wood components due to its potentially high selectivity and energy efficiency. The efficient recovery of hemicelluloses is of great interest because they are one of the main components of the dry wood tissue, constituting 20–30 wt% depending on the tree species (Sjöström, 1993). Hemicelluloses are generally degraded during Kraft pulping and are eventually combusted in the recovery

* Corresponding author.
E-mail address: tuve.mattsson@chalmers.se (T. Mattsson).
https://doi.org/10.1016/j.fbp.2021.04.009

Nomenclature

Roman

d	inner diameter of the gauge tube [m]
d_t	inner diameter of the nozzle throat [m]
dp	pressure drop over the FDG nozzle [Pa]
h	gauge height above a deposit [m]
h_o	gauge height above the membrane [m]
m_g	gauging mass flow rate [kg s^{-1}]
Re_{duct}	duct flow Reynolds number [–]

Greek

δ	fouling layer thickness [m]
μ	dynamic viscosity of the fluid [Pa s]
ρ	density of the fluid [kg m^{-3}]
τ_w	fluid shear stress [Pa]

Acronyms

ASL	acid-soluble lignin
CFV	cross-flow velocity [m s^{-1}]
DMSO	dimethylsulfoxide
FDG	fluid dynamic gauging
HPAEC	high-performance anion-exchange chromatography
LVDT	linear variable differential transformer
MF	microfiltration
MWCO	molecular weight cut-off
PSU	polysulfone
RI	refractive index
SEC	size-exclusion chromatography
STEX	steam explosion
TMP	transmembrane pressure
UF	ultrafiltration
UV	ultraviolet

boiler to generate energy, despite having a relatively low heating value (Sixta, 2006). It is potentially more beneficial to pre-extract the hemicelluloses as a raw material for bio-based products. The utilization of hemicelluloses to produce high value-added products have gained significant interest over the past years. Several studies have been conducted on the recovery of hemicelluloses by microfiltration (MF) and UF of spent sulfite liquors (Al-Rudainy et al., 2020) and process waters from thermomechanical and chemi-thermomechanical paper pulp mills (Persson and Jönsson, 2010; Thuvander et al., 2018; Thuvander and Jönsson, 2016). UF has also been carried out on hemicelluloses extracted from wheat bran using heat pretreatment (Arkell et al., 2013). The use of both dead-end filtration and MF as prefiltration methods preceding UF have been shown to result in a significant increase in flux (Krawczyk et al., 2013). Despite these developments, however, one of the biggest impediments that persist is membrane fouling.

Fouling limits the performance of membrane operations by increasing the flow resistance or by altering the selectivity of the membrane over time (Nagy, 2019). The build-up of materials on the surface of a membrane (i.e. cake formation) and within its pores (i.e. pore blockage) impairs the production capacity, as evidenced by flux decline. The fouling propensity during membrane operations is greatly influenced by membrane characteristics. Membrane morphology and hydrophilicity have been shown to influence the formation of fouling for regenerated cellulose and polyethersulfone membranes during the UF of process waters from chemi-thermomechanical pulp mills (Puro et al., 2010). In industrial operations involving membranes, careful selection of their properties, cleaning methods and operating conditions are implemented to maintain performance. These parameters must be considered if membrane separation is to be a viable option for biorefinery applications.

Membrane fouling behavior is difficult to predict and model. Contributing to this is the often limited characterization of the fouling deposits formed, which are based primarily on flux decline observations and composition changes of the permeate. Although various models for the build-up rate and properties of a fouling layer (e.g. particle capture (Broeckmann et al., 2006), inertial lift (Altena and Belfort, 1984; Drew et al., 1991) and shear-induced diffusivity (Davis and Leighton, 1987; Eckstein et al., 1977)) have been suggested, they are difficult to apply and are seldom utilized. The commonly used flux decline observations do not provide information on the thickness, composition and type of membrane fouling. Advanced methods that employ *in situ* real-time fouling investigations are therefore necessary to provide dynamic information of the fouling behavior and the properties of fouling layers formed. *In situ* methods for fouling investigations include direct observation (e.g. Marselina et al., 2008; Romero and Davis, 1991), laser-based techniques (e.g. Mendret et al., 2009; Schluep and Widmer, 1996), confocal laser scanning microscopy (e.g. Brans et al., 2007; Kromkamp et al., 2006), ultrasonic time domain reflectometry (e.g. Lin et al., 2013; Mairal et al., 1999), nuclear magnetic resonance imaging (e.g. Buetehorn et al., 2011; Yao et al., 1995), small angle scattering (e.g. David et al., 2008; Jin et al., 2014), electrical impedance spectroscopy (e.g. Coster et al., 1996; Sim et al., 2013) and fluid dynamic gauging (FDG). These methods have different operating principles, feed requirements, measurement capabilities and potential applications (Rudolph et al., 2019) so the selection of the method to be used is highly dependent on its cost, accuracy, operability and versatility (Lewis, 2015).

FDG offers information that cannot be obtained when other *in situ* methods are used. It not only provides an indication of the cake thickness as well as estimations of the cohesive and adhesive strengths of the fouling layer, but is also relatively inexpensive, requires minimal sample preparation, is highly versatile for different types of fluids and can be fully automated. FDG was first developed for making thickness measurements of soft deposits on solid surfaces (Tuladhar et al., 2000). The governing principle behind FDG is that the pressure drop due to flow through a constriction between a nozzle and a surface enables the simultaneous measurement of thickness and strength (Chew et al., 2004). FDG studies have been conducted on ballotini suspensions (Chew et al., 2007; Jones et al., 2010; Lister et al., 2011), yeast suspensions (Lewis et al., 2012) and, more recently, on forest-based samples such as Kraft lignin and microcrystalline cellulose (Lewis et al., 2017; Mattsson et al., 2015, 2018; Zhou et al., 2019; Zhou and Mattsson, 2019). The latter studies, however, focused mainly on the MF of model materials.

In this study, a method is developed using FDG to investigate the fouling behavior and shifts in fouling modes during cross-flow filtration of liquors extracted using steam explosion (STEX). The focus is on extending the use of FDG to complex, heterogeneous mixtures containing both particles and dissolved components and enabling *in situ* measurements at the transmembrane pressures (TMPs) used in the UF range, rather than developing a membrane separation system optimized

for hemicellulose production from STEX liquors. For this purpose, a membrane with small pores which was expected to yield considerable fouling was used. The characterizations of STEX liquor fractions were carried out using different analytical techniques to determine the properties of the samples collected. This work attempts to highlight how FDG could be used in characterizing the shifts in fouling modes to gain a better mechanistic understanding of the fouling behavior during membrane operations.

2. Experimental

2.1. Materials

Industrially cut softwood chips of mainly Norway spruce (*Picea abies*) (approx. 75%) and pine (*Pinus sylvestris*) (approx. 25%) sourced from a pulp mill in the southern part of Sweden were used as the raw material. These wood chips were air-dried at room temperature and sorted manually, including the removal of bark and knobs, to achieve a more uniform size distribution. The dimensions of the smallest wood chip were 17 mm × 20 mm × 2 mm ($L \times W \times H$) and those of the largest were 60 mm × 45 mm × 6 mm. The sorted wood chips served as the starting material for the mild STEX extraction.

Flat, permanently hydrophilic polysulfone (PSU) membranes (UFX10 pHt^{TM}, Alfa Laval) with a nominal molecular weight cut-off (MWCO) of 10 kDa, were mounted in a cross-flow filtration cell with an active membrane surface area of 2.4×10^{-3} m^2. The PSU membranes had a pure water flux of 412–466 L m^{-2} h^{-1} at 4 bar TMP, as specified by the manufacturer, and stored at room temperature inside a cupboard away from direct sunlight.

2.2. Extraction by mild steam explosion

Mild STEX at 7 bar (~165 °C) was performed for 20 min to extract a hemicellulose-rich fraction, thereby providing the feed material for the cross-flow UF. The STEX treatment conditions were kept mild to limit the degradation of wood components caused by acid hydrolysis (Jedvert et al., 2012). The pressure of the saturated steam was set at 7 bar, which was based on the investigations of different STEX conditions of Norway spruce by Jedvert et al. (2014), where the amount of the hemicellulose galactoglucomannan in the liquors was 23% of the total dry content after a 7 bar treatment.

The STEX liquor used in this study was prepared by first impregnating 500 g (dry basis) of softwood chips with deionized water in a vessel prior to steam treatment. A vacuum was then applied for 5 min, followed by pressurizing the vessel to 5 bar with nitrogen gas for 5 min to improve impregnation. The chips were left under pressure for 2–3 h while being immersed; the water was drained off thereafter, before the chips were placed in the steam explosion reactor. The reactor was heated with saturated steam, and the time was started when the desired pressure of 7 bar was attained. The pressure was maintained by continuously applying more steam for 20 min. The treatment was terminated by a sudden release of the pressure discharging the wood chips and the condensed steam. The STEX liquor and the steam-exploded wood chips were filtered through a Büchner funnel with a plastic grid mesh (< 1 mm openings) to separate the liquor from the solid wood chips. 1.5–2 L of STEX liquor, which contained dissolved wood components and small particles, was collected for every 500 g of wood chips processed. Two batches of STEX extraction liquors were mixed for each UF experiment. The STEX liquors were cooled to room temperature and then stored at 5 °C.

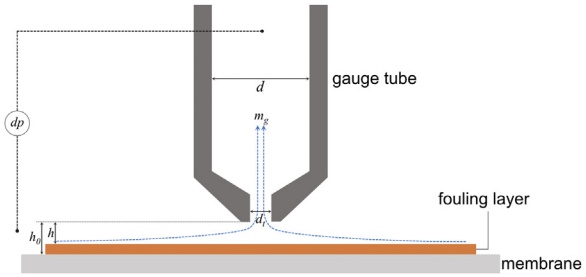

Fig. 1 – Schematic diagram of the FDG probe, where *dp* is the pressure drop over the FDG probe, m_g is the gauging mass flow rate, *d* is the inner diameter of the gauge tube (3 mm), d_t is the inner diameter of the nozzle throat (0.5 mm), h_o is the gauge height above the membrane and *h* is the gauge height above a deposit.

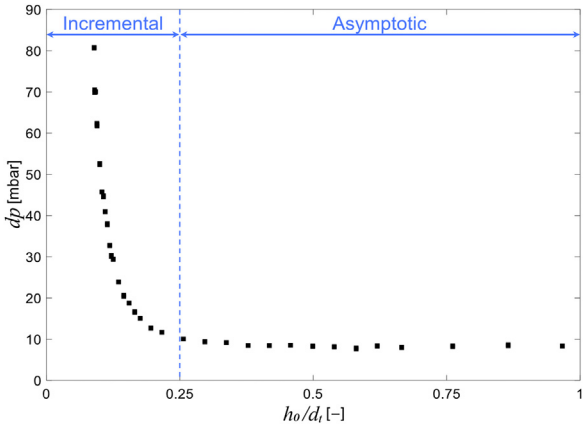

Fig. 2 – Example of an experimental *dp* vs. h_o/d_t where $h_o/d_t = 0.25$ marks the boundary between the incremental and the asymptotic zones ($d = 3$ mm, $d_t = 0.5$ mm, and $m_g = 0.1$ g s^{-1}).

2.3. Fluid dynamic gauging

Fluid dynamic gauging is an *in situ* monitoring technique that allows for the thickness, as well as the cohesive and adhesive strengths, of fouling layers to be estimated. It follows the fluid dynamic principle whereby a pressure drop is generated due to flow constriction between the tip of a nozzle and the top of a fouling layer, *h*, as presented in Fig. 1.

This study employs a pressure-mode FDG, where the thickness estimations are made by measuring the pressure drop, *dp*, over the FDG probe (inner diameters of the gauge tube, $d = 3$ mm, and nozzle throat, $d_t = 0.5$ mm) while fluid is withdrawn through the probe at a controlled gauging flow rate of $m_g = 0.1$ g s^{-1}. The fouling layer thickness, δ, is indicated by Eq. (1):

$$\delta = h_o - h \tag{1}$$

where h_o is the gauge height above the membrane and *h* is the gauge height above a deposit.

Fig. 2 shows the non-linear wall response from the FDG probe for a pristine membrane. At $h_o/d_t > 0.25$ (asymptotic zone), the *dp* values are low and relatively constant, while at $h_o/d_t \leq 0.25$ (incremental zone) the values increase rapidly as

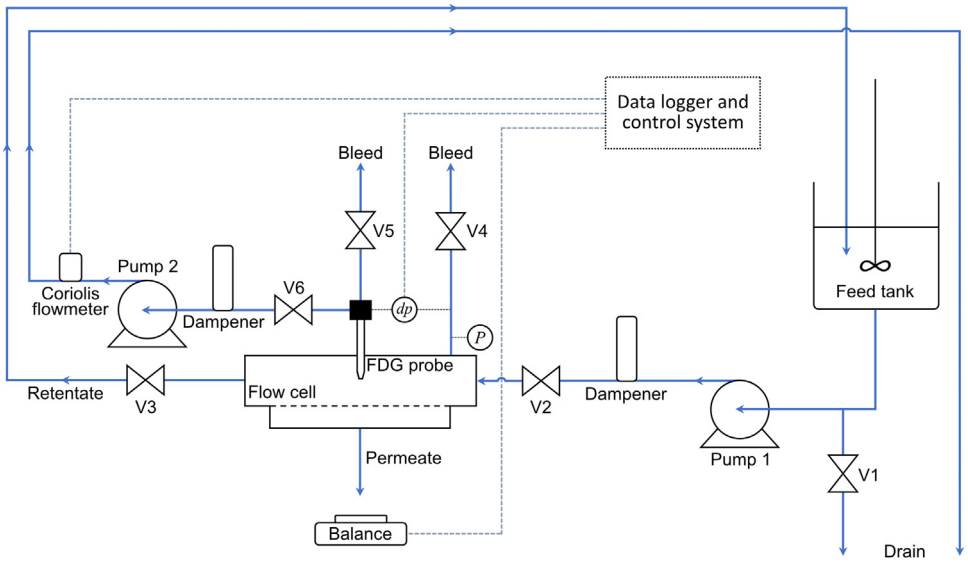

Fig. 3 – Schematic diagram of the cross-flow filtration test rig, including the feed and recirculation loops.

the probe approaches the membrane. This response relates the *dp* value to the distance of the probe from a surface. The thickness of the deposit is obtained by estimating *h* using the *dp* value at a known h_o.

Fluid shear stress is exerted on the surface of the fouling layer whilst FDG thickness measurements are being made. At elevated shear stress, loose fouling layers can be removed. This removal enables the cohesive and adhesive strengths of the layer to be estimated. Moving the probe closer to the fouling layer allows the successive removal of the layer to be tracked due to the increased applied shear stress. The maximum shear stress, $\tau_{w,max}$, can be estimated analytically via Eq. (2), with the assumption of creeping concentric flow between parallel plates:

$$\tau_{w,\max} = \frac{6\mu m_g}{\rho\pi h^2} \cdot \frac{1}{d_t} \tag{2}$$

where μ is the dynamic viscosity of the fluid and ρ is the density of the fluid. $\tau_{w,max}$ is in the region directly below the inner edge of the nozzle rim, at a radial distance $d_t/2$ from the centerline.

2.4. *Cross-flow filtration equipment*

All cross-flow filtration experiments were performed in a bench-scale, stainless-steel filtration test rig, as presented in Fig. 3, equipped with a flow cell and an FDG probe. The flow cell has a rectangular cross-section flow channel with dimensions of 150 mm × 16 mm × 15 mm. The FDG probe was positioned at the center of the flow channel; all thickness and strength measurements were made at this location to minimize possible rand effects close to the edges of the membranes (Mattsson et al., 2018). The probe can only be moved along the y-axis (i.e. vertical movements) and the fouling layer can only be investigated at that specific location.

The inlet of the flow cell is connected to a baffled feed tank (187 mm inner diameter, 5 L capacity) stirred by a pitched-blade impeller with two blades. The feed STEX liquor was circulated through the test section by a gear pump (Pump 1 in Fig. 3, GB-P35.PVS.A.B1, Ismatec), which maintained the desired cross-flow velocity (CFV). The TMP was measured by a pressure transducer (PXM419-010BA10V, Omega Engineering) and was regulated by the needle valve V3. The permeate was collected at atmospheric pressure and weighed on a precision balance (Quintix® 3102-1S, Sartorius) connected to a data-logging computer, while the retentate was recirculated back to the feed tank.

The vertical movement of the FDG probe was controlled by a stepper motor attached to a linear guide rail (Nanotec ST4209S1006-B) with a minimum linear movement of 0.31 μm. Its position was monitored by a potentiometer (534, Vishay Spectrol) and a linear variable differential transformer (LVDT) (SM-series LVDT, Singer Instruments) with an accuracy of ± 0.5 μm. The *dp* was measured by a differential pressure transducer (PX419-2.5DWUV, Omega Engineering) with an accuracy of ± 0.08% best fit straight line. The gauging mass flow rate during FDG measurements was maintained by a gear pump (Pump 2 in Fig. 3, DBS.11EEET2NMM104, Tuthill) and measured and controlled by a Coriolis flowmeter (Mini CORI-FLOW, Bronkhorst). A stainless-steel filter housing (Model 122, Headline Filters) was installed upstream of the Coriolis flowmeter as a prefilter to prevent clogging. All logged data from the LVDT and pressure transducers was monitored by a computer via LabView 2015 (National Instruments), with a detailed description of its automation presented elsewhere (Lewis, 2015).

2.5. *Filtration experiments*

The flat PSU membrane was initially swelled and rinsed by soaking it in deionized water at least a day prior to UF. The PSU membrane was then mounted in the filtration cell at the bottom of the cross-flow channel, a fresh membrane was used for each individual test series (referred to as runs 1, 2, 3, 4, 5 below). The position of the membrane was secured by mounting it on top of two supporting layers. A porous polypropylene sheet was placed directly underneath the membrane, which, in turn, was supported by a perforated stainless-steel slab with 2 mm diameter holes.

All filtration experiments were conducted with an initial feed STEX liquor volume of approximately 4 L. After storing at 5 °C for 1–3 days, the STEX liquor was heated under stirring at 40 °C to facilitate the dissolution of the wood components in the liquor. The STEX liquor was then placed in the baffled feed tank under continuous stirring. Its pH was unadjusted

at pH 3.7, and its temperature was cooled and maintained at 23–25 °C during UF. The CFV was set to ~0.07 m s^{-1} in all experiments, which corresponds to a duct flow Reynolds number Re_{duct} = ~1200 (i.e. laminar regime) in the cross-flow cell. The TMP was controlled at 2 bar (± 5%), with larger variations during the introduction of the STEX liquor feed stream or shortly thereafter. The permeate was collected using a permeate container on top of a precision balance, and the weight data was logged every two seconds to calculate the permeate flux while the FDG gauge flow was kept constant at 0.1 g s^{-1} during FDG measurements (i.e. "pressure-mode FDG").

For each run, the flow cell was cleaned by dismantling the system and washing each section with dishwasher detergent and water. Deionized water is recirculated for 0.5–1.0 h to ensure that the system is cleaned thoroughly prior to pure water flux determination.

2.5.1. FDG calibration

The FDG calibration data was taken from earlier work (Zhou et al., 2019; Zhou and Mattsson, 2019), where the probe position was verified by *dp* measurements at a known distance *h* from a surface using a solid plate instead of a membrane. The detailed description of the relationship of *dp* as a function of h/d_t is described in the supplementary material in Zhou et al. (2019), where the measured reference data was derived using the Curve Fitting Toolbox™ in MATLAB. At $h/d_t \leq 0.25$, the calibration data followed the master calibration curve in Eq. (3):

$$dp = c_1 \exp\left(\frac{c_2}{h/d_t}\right) + c_3 \exp\left(\frac{c_4}{h/d_t}\right) \quad (3)$$

where $c_1 = 1135$, $c_2 = -1.58$, $c_3 = 2.58$, $c_4 = 0.30$ and $R^2 = 0.99$.

2.5.2. Pure water flux and STEX liquor filtration

The pure water flux was verified first by circulating 5 L of deionized water at TMP = 2 bar, CFV = ~0.07 m s^{-1} for at least 1 h. This circulation of deionized water also facilitates the rinsing of the membrane while in operation. For each experiment, the exact position of the membrane was determined by moving the probe toward the membrane and noting the *dp* and h_o/d_t values. The membrane calibration curve was superimposed onto the master calibration curve, and the membrane position was confirmed when the membrane calibration measurements were adjusted with the *dp* and h_o offset values, $h_{o,offset}$ and $dp_{,offset}$, to overlap with the master calibration curve.

After determining the position of the membrane, the feed line was transferred from deionized water to the feed STEX liquor, and cross-flow UF was performed at the same conditions for at least 2 h. The FDG probe was retracted to the top of the flow cell (i.e. outside the LVDT range) to minimize disturbance of the fouling layer being formed. The gauge flow was also turned off to conserve the feed STEX liquor when no FDG measurements were being made, since the gauging liquid was not returned into the system. After an initial 30 or 45 min of fouling, FDG measurements were performed to investigate the fouling layer formed whilst the system was still subjected to UF of the STEX liquor. During FDG measurements, the fluid shear stress exerted by the probe can remove locally the whole, or a part of, the fouling layer directly below the nozzle rim of the probe. The probe is considered to make a low imprint, with a small diameter of ~1 mm, on the surface of the membrane, which reduces its influence on the flux curves.

The gauge tube is retracted after the first measurements have been made. The filtration operation continues for 30 or 45 min of additional fouling, when the fouling layer is allowed to redeposit on top of the membrane in the affected FDG zone. New measurements are conducted thereafter, and the fouling and measurement cycle is continued until at least 2 h of UF have elapsed. At the end of the UF, the permeate and retentate are collected for further analyses. It can be assumed that the feed concentration is constant, since the total volume of permeate (~100 mL) that was taken out of the system was low compared to the total volume of feed.

2.6. Analytical methods

High-performance anion-exchange chromatography (HPAEC), size-exclusion chromatography (SEC), Klason lignin and acid-soluble lignin (ASL) tests, total dry solids analysis and particle sizing by laser diffraction were all performed to characterize the properties of the STEX feed, retentate and membrane-fractionated permeates.

2.6.1. Laser diffraction and total dry solids of the feed material

The particle size distribution of the feed STEX liquor was analyzed by laser diffraction (Mastersizer 2000, Malvern Panalytical) with a detection range of 0.02–2000 μm. The size distribution was determined in three replicates for the heated STEX liquor and two replicates for the non-heated STEX liquor.

The total dry solids content of the feed STEX liquor was determined gravimetrically by freeze-drying. Six representative liquor samples were weighed and frozen using liquid nitrogen before placing them in the FreeZone® Triad™ Freeze Dry System.

2.6.2. Molecular weight determination

The molecular weight distribution of the streams was determined by SEC using dimethyl sulfoxide (DMSO) as eluent with the addition of 10 mM LiBr. Freeze-dried samples were dissolved in DMSO to a concentration of 1 mg mL^{-1}. The samples were filtered through a 0.2 μm syringe filter (GHP, Acrodisc) and then injected into a PL-GPC 50 Plus Integrated GPC System (Polymer Laboratories), equipped with PolarGel-M columns and refractive index (RI) and ultraviolet (UV) detectors. The calibration curve was generated from ten different molecular weights of pullulan using Cirrus GPC Version 3.2 software.

2.6.3. Klason lignin and acid-soluble lignin

Klason lignin, the insoluble residual material after hydrolysis using 72% sulfuric acid, can be quantified using gravimetric procedures established previously (Theander and Westerlund, 1986). Klason lignin also accounts for other acid-insoluble components present in the sample besides lignin. The ASL concentration was calculated from UV absorbance values of the hydrolysates measured at 205 nm using SPECORD® 205 (Analytik Jena), with a molar absorptivity constant of 110 L g^{-1} cm^{-1} (Lin and Dence, 1992).

2.6.4. Carbohydrate analysis

The hydrolysates from the analysis of Klason lignin were also used for the analysis of carbohydrates. The monomeric sugars present after hydrolysis of the STEX feed, permeate and retentate were quantified using a Dionex ICS-5000 HPLC system equipped with CarboPac™ PA1 columns, using NaOH and 0.2 M NaOH/NaAc as eluents. The Dionex HPAEC system

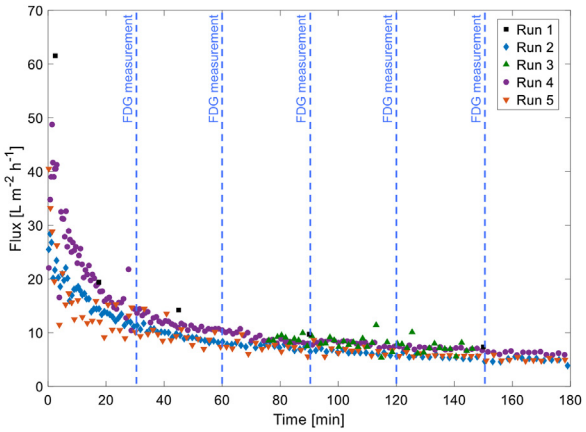

Fig. 4 – Flux vs. filtration time curves for Runs 1–5. Dashed lines: start of the 30 min time interval FDG measurements. N.B. Run 1 had time intervals of 45 min.

employs a pulsed amperometric detector and operates using Chromeleon 7 software (Chromatography Data System, Version 7.1.0.898).

3. Results and discussion

Five cross-flow UF experiments were conducted to characterize fouling behavior. The following sections include the permeate flux profiles, *dp* vs. h/d_t curves, total dry solids content, particle size distribution, carbohydrate and lignin analyses and the molecular weight distribution of the membrane-fractionated samples.

3.1. *Flux profiles*

The superimposed flux curves of the cross-flow experiments are presented in Figs. S1 and 4, which show the pure water flux values and the permeate flux decline of the fouled PSU membrane, respectively. The TMP was maintained at 2 bar for all experiments, with a 5% error margin.

The pure water flux values, shown in Fig. S1, displayed a relatively broad range between the individual experiments (160–360 $L\,m^{-2}\,h^{-1}$). Such variation could indicate the presence of varying amounts of residual foulants from earlier runs even after the system had been cleaned, which is consistent with the observations of Zhou and Mattsson (2019), made on a system with microcrystalline cellulose particles using the same experimental rig as the present study. However, the differences in the initial flux in this study appear to have had a minimal influence on the flux and its decline behavior during UF of the STEX liquor, as can be seen in Fig. 4.

A severe decline in the permeate flux values was observed at the start of the feed change from deionized water to STEX liquor: the flux values dropped to less than 15 $L\,m^{-2}\,h^{-1}$ at the initial FDG measurement time. The permeate flux declined gradually, attaining lower and steadier flux values at the latter part of the filtration. The permeate flux decline during UF of STEX liquors followed a consistent trend, with flux values of < 10 $L\,m^{-2}\,h^{-1}$ after 120 min of filtration. The permeate flux values for Runs 2, 3, 4 and 5 were 5.6, 8.0, 7.4 and 5.7 $L\,m^{-2}\,h^{-1}$, respectively.

The permeate flux values for Run 1 were calculated manually, based on the permeate collected for longer time intervals because a less precise permeate collection balance was used in this particular experiment (PB3002-S, Mettler Toledo). Only flux values beyond 75 min were considered for Run 3 due to unstable weight readings caused by the flow cell permeate tube contacting the permeate container during the initial part of the UF. It is worth noting that the flux curves were not affected by the FDG probe measurements since the impact area of the probe was very small compared to the total membrane area.

The results of the permeate flux curves suggest the presence of severe fouling, where the pores of the PSU membrane may also be blocked in various modes (Hermans and Bredée, 1936; Hermia, 1982). However, from the flux curves alone, it is very difficult to build a deeper understanding of the contribution of different fouling mechanisms (e.g. cake formation and pore blockage), especially if these fouling modes take place simultaneously.

3.2. *FDG profiles*

Fig. 5 shows the *dp* vs. h/d_t profiles for the cross-flow filtration experiments with FDG measurements, where an increase in *dp* further away from the pristine membrane corresponds to a thicker fouling layer. These plots have been corrected with $h_{o,offset}$ and $dp_{,offset}$. The normalized fouling thickness (δ/d_t) can be estimated as the shift on the x-axes required to overlap the pristine membrane data points with corresponding fouling data. The pristine membrane curves (■) showed a consistent trend: the *dp* values remained constant at the baseline level in the asymptotic zone ($h_o/d_t > 0.25$) but a sharp increase was measured in the incremental zone ($h_o/d_t < 0.25$), indicating that the probe was positioned closer to the membrane. FDG measurements were terminated once the pressure drop reached 100 mbar.

A consistent trend that was noticed between experiments is that the initial measurement for each experiment displays the thickest deposit, while the remeasurements reveal surface deposits that become continually thinner. This trend illustrates how FDG could be used to track the way in which thinner fouling layers were deposited on the refouled, non-pristine membrane compared to the initial layer formed on the pristine membrane. For Runs 1, 3 and 4, the later FDG remeasurements almost follow the pristine membrane curve (with slight divergence at higher *dp* values), indicating the absence of a surface fouling layer that could withstand the minimum applied shear stress (approx. 34 Pa). Although the remeasured FDG profiles in Runs 2 (Fig. 5b) and 5 (Fig. 5e) indicate thinner deposits, the response is shifted to the right for all fouling measurements with the exception of the pristine membrane curve. While it cannot be ruled out that this shift is caused by thicker deposits right under the probe, the resilience of the shift during repeated destructive FDG measurements suggests that the membrane position might have moved during operation, above its known position from the pristine membrane curve. The cause of this possible movement is uncertain, but it may have occurred whilst the feed material was being changed, which is where a surge in TMP was noted.

Upon a closer inspection of the FDG profiles, it can be observed that the profiles measured during fouling of the system typically increase more sharply than the response of the membrane in a clean system. The measurements during fouling do not converge toward the response for the membrane measurements at low probe clearing heights, which would be expected whilst the fouling layer was being removed by the probe. This effect may be caused by the entrapment

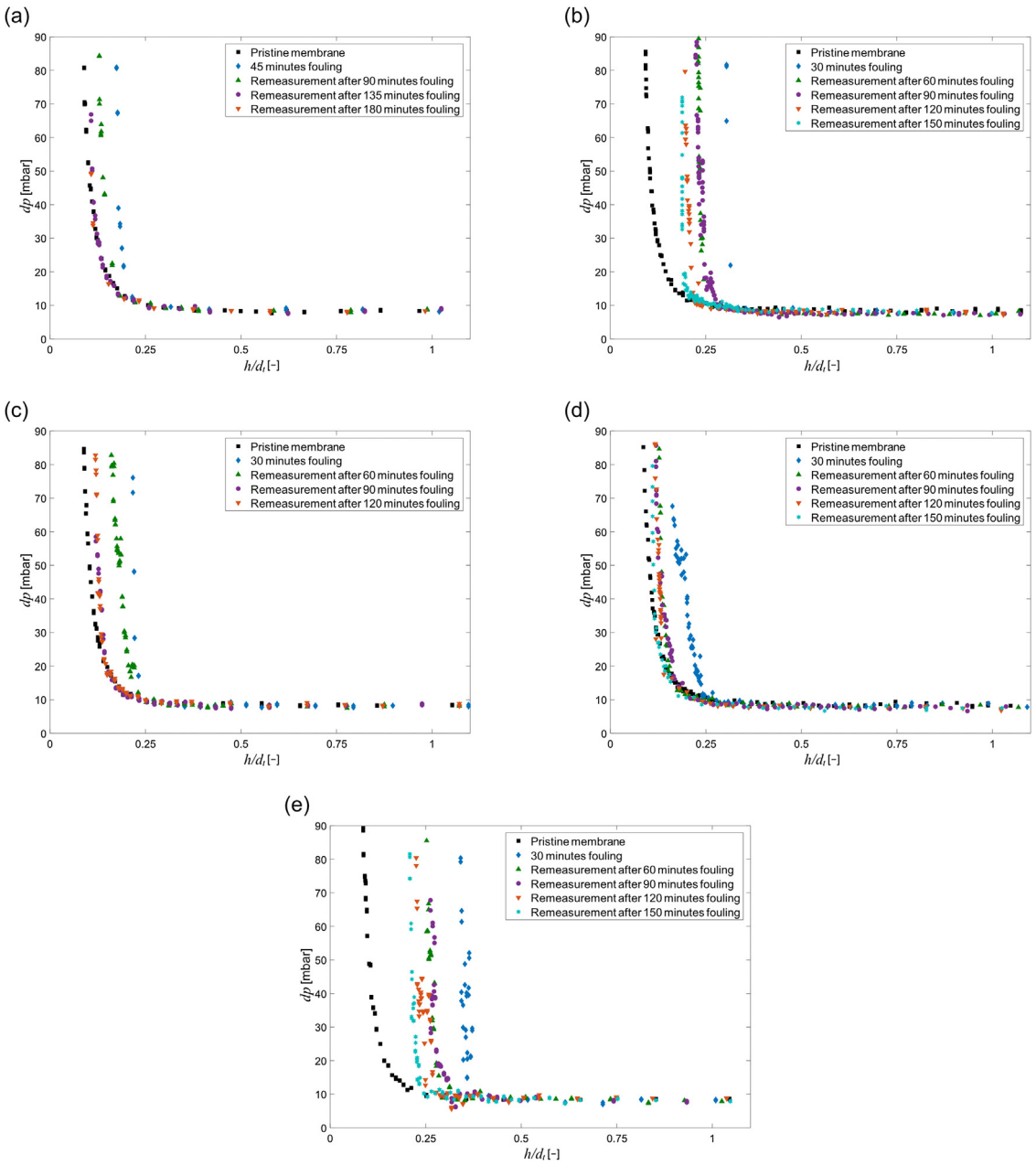

Fig. 5 – Differential pressure *dp* over the FDG nozzle vs. h/d_t measured during cross-flow filtration using a 10 kDa PSU membrane at 2 bar TMP, where (a) is Run 1, (b) is Run 2, (c) is Run 3, (d) is Run 4 and (e) is Run 5. N.B. The *x*-axis for the pristine membrane curve (■) is h_o/d_t due to the absence of a fouling layer.

of particles in the feed between the tip of the FDG probe and the fouling layer/membrane surface. The entrapment of particles is further supported by the observation that, as the probe was positioned close to the surface (< 100 μm), the *dp* still increases even at a constant probe position. In certain instances, the *dp* also drops suddenly, which may be due to the foulants being dislodged from underneath the probe tip. This entrapment, that occurred during the measurements, hindered estimations of the strength properties of the fouling layer from being made and highlighted the difficulty encountered in capturing the actual thickness of the fouling layer formed. For a preliminary experiment during MF of STEX liquors, a similar trend with a sharper increase for the fouled system compared to the pristine membrane could also be observed (results not included), indicating that the same challenge is present in that system as well.

The results from both the flux and the *dp* vs. h/d_t profiles provide information about the fouling behavior and the relationship between the development of a cake fouling layer (i.e. surface fouling) and internal fouling due to pore blocking of the membrane. Here, FDG showed how surface fouling was more prevalent during the initial fouling stage and less so during refouling, when more internal fouling would have been formed. The presence of multiple fouling mechanisms often makes the identification of the predominant mechanism based on flux decline alone difficult (e.g. Nataraj et al., 2008). Nevertheless, these results show that FDG offers an additional tool that can also be very useful for complex, heterogeneous systems. For future work, it would also be interesting to study the fouling behavior of STEX liquors in the MF range for this feed and investigate if severe fouling would also be observed and if a shift in fouling modes would occur.

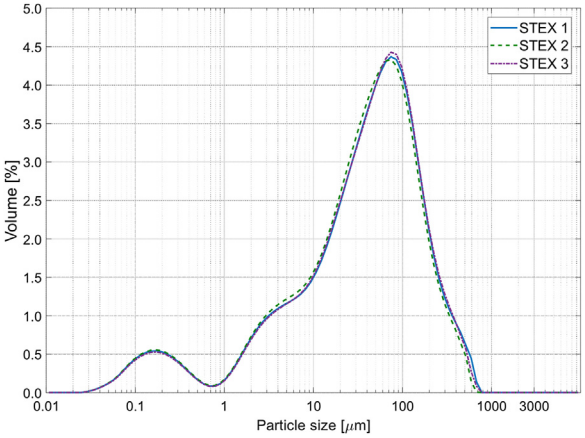

Fig. 6 – Size distribution of the feed STEX liquor heated under stirring at 40 °C, showing the volume-based particle distribution in logarithmic scale.

3.3. *Characterization of feed and collected fractions*

The total dry solids of the feed and permeate STEX liquors were determined by gravimetry. Six samples were used, in which around 8.4 mg in total dry solids were found to be present in every g of feed STEX liquor. The total amount of dry solids in the permeate was estimated to be in the range of 2–5 mg/g of permeate, based on the permeate collected and freeze-dried from Runs 1 and 3.

3.3.1. *Particle size distribution*

Fig. 6 shows the volume-based size distribution of the particles and agglomerates in the feed STEX liquor after being heated to 40 °C under stirring (i.e. the treatment is performed after storage and before filtration of the sample). Two distinct peaks were detected at approximately 0.2 μm and 70 μm ($D_{(10)}$: 2.3 μm; $D_{(50)}$: 43.1 μm; $D_{(90)}$: 183.8 μm) based on the size distribution curves of three repeated measurements from the same feed material. Similar distribution curves were obtained for a feed STEX liquor sample that was stirred at room temperature (~20 °C), as presented in Fig. S2.

3.3.2. *Molecular weight distribution*

The molecular weight distributions of fractions from Runs 1, 2, 4 and 5 from the UV detector, using the SEC system described above, are presented in Table S2. The DMSO-based SEC system was purposed for lignin-rich streams and not optimized for the relatively hemicellulose-rich STEX fractions. Still, a decrease in the weight average molecular weight, M_w, by 400–500 Da is observed for the permeate compared to the feed and retentate, indicating that smaller species passed through the 10 kDa PSU membrane while larger components were retained. The polydispersity, M_w/M_n, of the feed STEX liquor also decreased as its components passed through the membrane. A decline in polydispersity is expected since the PSU membrane would retain a higher molecular weight fraction. The signal from the RI detector was very weak: only a peak corresponding to a very low molecular fraction (M_w of 180 Da) could be identified. This peak was present to the same extent in all samples (feeds, retentates and permeates) and corresponds to an M_w much lower than the MWCO. However, due to the weak signal, no conclusion could be drawn from this.

3.3.3. *Composition*

Tables 1, S3 and S4 show the results of the carbohydrate and lignin analyses for streams in Runs 1–5. The values are given in wt% of the dried sample after the streams that were collected were freeze-dried. The analyzed fractions mostly contained mannose, arabinose and Klason lignin. The composition of the feed STEX liquor was consistent with results obtained in earlier work (Mattsson et al., 2017). The trend of an increase in arabinose content and a decrease in mannose content in the permeate stream is also in line with earlier observations made during membrane fractionation of STEX liquor (Mattsson et al., 2017). It can be noted that arabinose, as a side chain of the hemicellulose xylan, is vulnerable to autohydrolysis and can be cleaved from the backbone, forming smaller species that can be expected to accumulate in the permeate. It is likely that the other components present in the STEX liquor fractions, and account for some of the remaining percentage of the composition, originate from dissolved extractives (Wojtasz-Mucha et al., 2019), fatty acids and other organic compounds present in the wood samples (Jedvert et al., 2014).

In Run 3, the permeates were collected at different time intervals to determine whether or not there is a shift in composition as the severity of fouling increases. The results obtained showed no significant difference in the composition of the collected permeates based on their monomeric sugars, Klason lignin and ASL content, as shown in Table S4. While the focus of this study was on the development of the FDG characterization method, a deeper investigation of the chemical characteristics of the fractions as well as the particles present

Table 1 – Anhydrosugar composition and lignin content of the membrane-fractionated STEX liquor samples for Runs 1, 2, 4, 5 and the sample used to determine the particle size distrubution reported in Fig. 6 [wt %].

Sample	Run No.	Arabinose	Galactose	Glucose	Xylose	Mannose	Klason lignin	ASL	Total
Feed STEX liquor	1	8.9	5.4	5.8	6.5	20	12.4	2.5	61.5
Feed STEX liquor[a]		10.1	6.2	6.5	7.5	23.2	14.7	3.3	71.5
Permeate		15.3	5.6	4.2	9.7	15.8	12	3.5	66.1
Feed STEX liquor	2	9.4	5.3	6.5	7.3	20.7	13.3	3.5	66
Retentate		9	5.1	6	7.2	20.5	13	3.2	64
Permeate[a]		16.5	4.8	3.4	8	12.7	10.9	5.8	62.1
Feed STEX liquor	4	8.3	5.7	6.8	8	24.5	11	3.2	67.5
Retentate		8.2	5.6	6.7	7.8	23.5	16.3	3.1	71.2
Permeate		10.7	4.9	5.3	9.1	20.5	8.6	4.2	63.3
Retentate	5	8.3	5.5	6.7	7.7	23.5	11	2.8	65.5
Permeate		11	5.3	5.7	8.8	21.3	9.4	4	65.5

[a] Calculated average of two measurements. The results from the individual measurements can be found in Table S3 in the Supplementary Material.

in the feed is of interest and will be a focus in future investigations.

4. Conclusions

In this study, the fouling behavior during cross-flow filtration of steam explosion (STEX) liquors was investigated using fluid dynamic gauging (FDG). The aim was to develop an FDG method that would be applicable to heterogeneous streams of extracted wood components at the transmembrane pressures (TMPs) used in the UF range, rather than developing a membrane separation system optimized for hemicellulose production from STEX liquors.

The STEX liquor fraction collected after the mild STEX pretreatment at 7 bar contained not only dissolved wood components but also small particles. Cross-flow filtration of the STEX liquor, using 10 kDa polysulfone membranes at 2 bar transmembrane pressure, showed a severe decline in permeate flux. During the first 120 min of filtration, the average flux dropped to around $7\,L\,m^{-2}\,h^{-1}$. A challenge when applying FDG measurements to this system was the entrapment of particles from the feed between the tip of the FDG probe and the membrane which likely occurred and made it difficult to precisely determine the thickness and strength properties of the fouling layer formed. However, based on the FDG profiles of the filtration experiments, it could be observed that thicker surface fouling layers were formed during the initial stages of filtration on a pristine membrane compared to subsequent fouling on the refouled, non-pristine membrane, onto which thinner layers were deposited. At later filtration times (> 120 min), the reformed surface layers were typically so thin and weak that they could not withstand the minimum shear stress applied during the FDG measurements. These FDG results yield information on the relationship between surface fouling, i.e. the formation of a cake layer, versus internal fouling due to pore blocking of the membrane. For the system investigated, FDG showed how surface fouling was prevalent during the initial fouling stage while later on in the operation, when more internal fouling had been formed, thinner/weaker surface deposits were reformed if the layer was disturbed.

The method developed, using FDG for investigating the fouling behavior of wood components extracted using a mild STEX pretreatment, highlights how FDG can be used to gain a better mechanistic understanding of the fouling behavior during membrane operations.

CRediT Author statement

Kenneth Arandia: investigation, methodology, data curation, formal analysis, visualization, writing – original draft, writing – review & editing.

Upasna Balyan: investigation.

Tuve Mattsson: supervision, conceptualization, writing – review & editing, resources, project administration, funding acquisition.

Declaration of Competing Interest

The authors report no declarations of interest.

Acknowledgements

The authors would like to thank the Knut and Allice Wallenberg Foundation, through the Wallenberg Wood Science Center (WWSC), and theÅForsk Foundationfor their financial support. Alfa Laval is also acknowledged for providing the hydrophilic PSU membranes. Special thanks are due to Mr. Anders Ahlbom for his assistance during SEC analysis.

Appendix A. Supplementary data

Supplementary material related to this article can be found, in the online version, at https://doi.org/10.1016/j.fbp.2021.04.009.

References

Al-Rudainy, B., Galbe, M., Wallberg, O., 2020. From lab-scale to on-site pilot trials for the recovery of hemicellulose by ultrafiltration: Experimental and theoretical evaluations. Sep. Purif. Technol. 250, 117187, http://dx.doi.org/10.1016/j.seppur.2020.117187.

Altena, F.W., Belfort, G., 1984. Lateral migration of spherical particles in porous flow channels: application to membrane filtration. Chem. Eng. Sci. 39, 343–355, http://dx.doi.org/10.1016/0009-2509(84)80033-0.

Arkell, A., Krawczyk, H., Jönsson, A.-S., 2013. Influence of heat pretreatment on ultrafiltration of a solution containing hemicelluloses extracted from wheat bran. Sep. Purif. Technol. 119, 46–50, http://dx.doi.org/10.1016/j.seppur.2013.09.001.

Brans, G., van Dinther, A., Odum, B., Schroën, C.G.P.H., Boom, R.M., 2007. Transmission and fractionation of micro-sized particle suspensions. J. Memb. Sci. 290, 230–240, http://dx.doi.org/10.1016/j.memsci.2006.12.045.

Broeckmann, A., Busch, J., Wintgens, T., Marquardt, W., 2006. Modeling of pore blocking and cake layer formation in membrane filtration for wastewater treatment. Desalination 189, 97–109, http://dx.doi.org/10.1016/j.desal.2005.06.018.

Buetehorn, S., Utiu, L., Küppers, M., Blümich, B., Wintgens, T., Wessling, M., Melin, T., 2011. NMR imaging of local cumulative permeate flux and local cake growth in submerged microfiltration processes. J. Memb. Sci. 371, 52–64, http://dx.doi.org/10.1016/j.memsci.2011.01.018.

Chew, J.Y.M., Paterson, W.R., Wilson, D.I., 2004. Fluid dynamic gauging for measuring the strength of soft deposits. J. Food Eng. 65, 175–187, http://dx.doi.org/10.1016/j.jfoodeng.2004.01.013.

Chew, Y.M.J., Paterson, W.R., Wilson, D.I., 2007. Fluid dynamic gauging: a new tool to study deposition on porous surfaces. J. Memb. Sci. 296, 29–41, http://dx.doi.org/10.1016/j.memsci.2007.03.009.

Coster, H.G.L., Chilcott, T.C., Coster, A.C.F., 1996. Impedance spectroscopy of interfaces, membranes and ultrastructures. In: Bioelectrochemistry and Bioenergetics. Elsevier Science S.A., pp. 79–98, http://dx.doi.org/10.1016/0302-4598(96)05064-7.

David, C., Pignon, F., Narayanan, T., Sztucki, M., Gésan-Guiziou, G., Magnin, A., 2008. Spatial and temporal in situ evolution of the concentration profile during casein micelle ultrafiltration probed by small-angle X-ray scattering. Langmuir 24, 4523–4529, http://dx.doi.org/10.1021/la703256s.

Davis, R.H., Leighton, D.T., 1987. Shear-induced transport of a particle layer along a porous wall. Chem. Eng. Sci. 42, 275–281, http://dx.doi.org/10.1016/0009-2509(87)85057-1.

Drew, D.A., Schonberg, J.A., Belfort, G., 1991. Lateral inertial migration of a small sphere in fast laminar flow through a membrane duct. Chem. Eng. Sci. 46, 3219–3224, http://dx.doi.org/10.1016/0009-2509(91)85023-Q.

Eckstein, E.C., Bailey, D.G., Shapiro, A.H., 1977. Self-diffusion of particles in shear flow of a suspension. J. Fluid Mech. 79, 191–208, http://dx.doi.org/10.1017/S0022112077000111.

Hermans, P.H., Bredée, H.L., 1936. Principles of the mathematical treatment of constant-pressure filtration. J. Soc. Chem. Ind., T1–T4.
Hermia, J., 1982. Constant pressure filtration laws – application to power law non-Newtonian fluids. Trans. Inst. Chem. Eng. 60, 183–187.
Jedvert, K., Hasani, M., Wells Jr., T., Theliander, H., 2014. Analyses of wood components in mild steam explosion liquors from spruce. Nord. Pulp Pap. Res. J. 29, 557–566, http://dx.doi.org/10.3183/npprj-2014-29-04-p557-567.
Jedvert, K., Saltberg, A., Lindström, M., Theliander, H., 2012. Mild steam explosion and chemical pre-treatment of Norway spruce. Bioresources 7, 2051–2074.
Jin, Y., Hengl, N., Baup, S., Pignon, F., Gondrexon, N., Sztucki, M., Gésan-Guiziou, G., Magnin, A., Abyan, M., Karrouch, M., Blésès, D., 2014. Effects of ultrasound on cross-flow ultrafiltration of skim milk: Characterization from macro-scale to nano-scale. J. Memb. Sci. 470, 205–218, http://dx.doi.org/10.1016/j.memsci.2014.07.043.
Jones, S.A., Chew, Y.M.J., Bird, M.R., Wilson, D.I., 2010. The application of fluid dynamic gauging in the investigation of synthetic membrane fouling phenomena. Food Bioprod. Process. 88, 409–418, http://dx.doi.org/10.1016/j.fbp.2010.07.004.
Krawczyk, H., Arkell, A., Jönsson, A.-S., 2013. Impact of prefiltration on membrane performance during isolation of hemicelluloses extracted from wheat bran. Sep. Purif. Technol. 116, 192–198, http://dx.doi.org/10.1016/j.seppur.2013.05.039.
Kromkamp, J., Faber, F., Schroen, K., Boom, R., 2006. Effects of particle size segregation on crossflow microfiltration performance: control mechanism for concentration polarisation and particle fractionation. J. Memb. Sci. 268, 189–197, http://dx.doi.org/10.1016/j.memsci.2005.06.012.
Lewis, W., 2015. Advanced Studies of Membrane Fouling Investigation of Cake Fouling Using Fluid Dynamic Gauging. University of Bath.
Lewis, W.J.T., Chew, Y.M.J., Bird, M.R., 2012. The application of fluid dynamic gauging in characterising cake deposition during the cross-flow microfiltration of a yeast suspension. J. Memb. Sci. 405–406, 113–122, http://dx.doi.org/10.1016/j.memsci.2012.02.065.
Lewis, W.J.T., Mattsson, T., Chew, Y.M.J., Bird, M.R., 2017. Investigation of cake fouling and pore blocking phenomena using fluid dynamic gauging and critical flux models. J. Memb. Sci. 533, 38–47, http://dx.doi.org/10.1016/j.memsci.2017.03.020.
Lin, S., Dence, C., 1992. Methods in Lignin Chemistry. Springer Series in Wood Science.
Lin, Y.H., Tung, K.L., Wang, S.H., Zhou, Q., Shung, K.K., 2013. Distribution and deposition of organic fouling on the microfiltration membrane evaluated by high-frequency ultrasound. J. Memb. Sci. 433, 100–111, http://dx.doi.org/10.1016/j.memsci.2013.01.020.
Lister, V.Y., Lucas, C., Gordon, P.W., Chew, Y.M.J., Wilson, D.I., 2011. Pressure mode fluid dynamic gauging for studying cake build-up in cross-flow microfiltration. J. Memb. Sci. 366, 304–313, http://dx.doi.org/10.1016/j.memsci.2010.10.017.
Mairal, A.P., Greenberg, A.R., Krantz, W.B., Bond, L.J., 1999. Real-time measurement of inorganic fouling of RO desalination membranes using ultrasonic time-domain reflectometry. J. Memb. Sci. 159, 185–196, http://dx.doi.org/10.1016/S0376-7388(99)00058-7.
Marselina, Y., Le-Clech, P., Stuetz, R., Chen, V., 2008. Detailed characterisation of fouling deposition and removal on a hollow fibre membrane by direct observation technique. Desalination 231, 3–11, http://dx.doi.org/10.1016/j.desal.2007.11.033.
Mattsson, T., Azhar, S., Eriksson, S., Helander, M., Henriksson, G., Jedvert, K., Lawoko, M., Lindström, M., McKee, L., Oinonen, P., Westerberg, N., Theliander, H., 2017. The development of a wood-based materials – biorefinery. Bioresources 12, 9152–9182.
Mattsson, T., Lewis, W.J.T., Chew, Y.M.J., Bird, M.R., 2018. The use of fluid dynamic gauging in investigating the thickness and cohesive strength of cake fouling layers formed during cross-flow microfiltration. Sep. Purif. Technol. 198, 25–30, http://dx.doi.org/10.1016/j.seppur.2017.01.040.
Mattsson, T., Lewis, W.J.T., Chew, Y.M.J., Bird, M.R., 2015. In situ investigation of soft cake fouling layers using fluid dynamic gauging. Food Bioprod. Process. 93, 205–210, http://dx.doi.org/10.1016/j.fbp.2014.09.003.
Mendret, J., Guigui, C., Schmitz, P., Cabassud, C., 2009. In situ dynamic characterisation of fouling under different pressure conditions during dead-end filtration: compressibility properties of particle cakes. J. Memb. Sci. 333, 20–29, http://dx.doi.org/10.1016/j.memsci.2009.01.035.
Nagy, E., 2019. Basic Equations of Mass Transport through a Membrane Layer, 2nd ed. Elsevier.
Nataraj, S., Schomäcker, R., Kraume, M., Mishra, I.M., Drews, A., 2008. Analyses of polysaccharide fouling mechanisms during crossflow membrane filtration. J. Memb. Sci. 308, 152–161, http://dx.doi.org/10.1016/j.memsci.2007.09.060.
Persson, T., Jönsson, A.-S., 2010. Isolation of hemicelluloses by ultrafiltration of thermomechanical pulp mill process water – influence of operating conditions. Chem. Eng. Res. Des. 88, 1548–1554, http://dx.doi.org/10.1016/j.cherd.2010.04.002.
Puro, L., Kallioinen, M., Mänttäri, M., Natarajan, G., Cameron, D.C., Nyström, M., 2010. Performance of RC and PES ultrafiltration membranes in filtration of pulp mill process waters. Desalination 264, 249–255, http://dx.doi.org/10.1016/j.desal.2010.06.034.
Ragauskas, A.J., Williams, C.K., Davison, B.H., Britovsek, G., Cairney, J., Eckert, C.A., Frederick, W.J., Hallett, J.P., Leak, D.J., Liotta, C.L., Mielenz, J.R., Murphy, R., Templer, R., Tschaplinski, T., 2006. The path forward for biofuels and biomaterials. Science (80-) 311, 484–489, http://dx.doi.org/10.1126/science.1114736.
Romero, C.A., Davis, R.H., 1991. Experimental verification of the shear-induced hydrodynamic diffusion model of crossflow microfiltration. J. Memb. Sci. 62, 249–273, http://dx.doi.org/10.1016/0376-7388(91)80042-5.
Rudolph, G., Virtanen, T., Ferrando, M., Güell, C., Lipnizki, F., Kallioinen, M., 2019. A review of in situ real-time monitoring techniques for membrane fouling in the biotechnology, biorefinery and food sectors. J. Memb. Sci., http://dx.doi.org/10.1016/j.memsci.2019.117221.
Schluep, T., Widmer, F., 1996. Initial transient effects during cross flow microfiltration of yeast suspensions. J. Memb. Sci. 115, 133–145, http://dx.doi.org/10.1016/0376-7388(95)00321-5.
Sim, L.N., Wang, Z.J., Gu, J., Coster, H.G.L., Fane, A.G., 2013. Detection of reverse osmosis membrane fouling with silica, bovine serum albumin and their mixture using in-situ electrical impedance spectroscopy. J. Memb. Sci. 443, 45–53, http://dx.doi.org/10.1016/j.memsci.2013.04.047.
Sixta, H., 2006. Handbook of Pulp. WILEY-VCH Verlag GmbH & Co. KGaA, Weinheim.
Sjöström, E., 1993. Wood Chemistry Fundamentals and Applications, 2nd ed. Academic Press, San Diego, CA, USA.
Theander, O., Westerlund, E.A., 1986. Studies on dietary fiber. 3. Improved procedures for analysis of dietary fiber. J. Agric. Food Chem. 34, 330–336, http://dx.doi.org/10.1021/jf00068a045.
Thuvander, J., Jönsson, A.-S., 2016. Extraction of galactoglucomannan from thermomechanical pulp mill process water by microfiltration and ultrafiltration-Influence of microfiltration membrane pore size on ultrafiltration performance. Chem. Eng. Res. Des. 105, 171–176, http://dx.doi.org/10.1016/j.cherd.2015.12.003.
Thuvander, J., Zarebska, A., Hélix-Nielsen, C., Jönsson, A.-S., 2018. Characterization of irreversible fouling after ultrafiltration of thermomechanical pulp mill process water. J. Wood Chem. Technol. 38, 276–285, http://dx.doi.org/10.1080/02773813.2018.1454962.
Tuladhar, T.R., Paterson, W.R., Macleod, N., Wilson, D.I., 2000. Development of a novel non-contact proximity gauge for thickness measurement of soft deposits and its application in fouling studies. Can. J. Chem. Eng. 78, 935–947, http://dx.doi.org/10.1002/cjce.5450780511.

Uragami, T., 2017. Science and Technology of Separation Membranes. John Wiley & Sons, Inc.
Wojtasz-Mucha, J., Mattsson, C., Hasani, M., Theliander, H., 2019. Pretreatment and cooking of forest residues. Bioresources 14, 9454–9471, http://dx.doi.org/10.15376/biores.14.4.9454-9471.
Yao, S., Costello, M., Fane, A.G., Pope, J.M., 1995. Non-invasive observation of flow profiles and polarisation layers in hollow fibre membrane filtration modules using NMR micro-imaging. J. Memb. Sci. 99, 207–216, http://dx.doi.org/10.1016/0376-7388(94)00219-O.
Zhou, M., Mattsson, T., 2019. Effect of crossflow regime on the deposit and cohesive strength of membrane surface fouling layers. Food Bioprod. Process. 115, 185–193, http://dx.doi.org/10.1016/j.fbp.2019.03.013.
Zhou, M., Sandström, H., Belioka, M.P., Pettersson, T., Mattsson, T., 2019. Investigation of the cohesive strength of membrane fouling layers formed during cross-flow microfiltration: The effects of pH adjustment on the properties and fouling characteristics of microcrystalline cellulose. Chem. Eng. Res. Des. 149, 52–64, http://dx.doi.org/10.1016/j.cherd.2019.06.037.